Applied Catalysis B: Environmental 132–133 (2013) 28–38

Contents lists available at SciVerse ScienceDirect

Applied Catalysis B: Environmental

journal homepage: www.elsevier.com/locate/apcatb

Nanostructured Pd modified Ni/CeO_2 catalyst for water gas shift and catalytic hydrogen combustion reaction

Vijay M. Shinde, Giridhar Madras*

Department of Chemical Engineering, Indian Institute of Science, Bangalore-560 012, India

ARTICLE INFO

Article history:
Received 5 September 2012
Received in revised form 31 October 2012
Accepted 16 November 2012
Available online 24 November 2012

Keywords:
Solution combustion
Ceria-supported catalyst
CO methanation
Redox mechanism

ABSTRACT

Nanostructured Pd-modified Ni/CeO_2 catalyst was synthesized in a single step by solution combustion method and characterized by XRD, TEM, XPS, TPR and BET surface analyzer techniques. The catalytic performance of this compound was investigated by performing the water gas shift (WGS) and catalytic hydrogen combustion (CHC) reaction. The present compound is highly active and selective (100%) toward H_2 production for the WGS reaction. A lack of CO methanation activity is an important finding of present study and this is attributed to the ionic substitution of Pd and Ni species in CeO_2. The creation of oxide vacancies due to ionic substitution of aliovalent ions induces dissociation of H_2O that is responsible for the improved catalytic activity for WGS reaction. The combined H_2-TPR and XPS results show a synergism exists among Pd, Ni and ceria support. The redox reaction mechanism was used to correlate experimental data for the WGS reaction and a mechanism involving the interaction of adsorbed H_2 and O_2 through the hydroxyl species was proposed for CHC reaction. The parity plot shows a good correspondence between the experimental and predicted reaction rates.

1. Introduction

<Hydrogen is considered as the most efficient and environmentally benign energy fuel. It allows additional flexibility in the selection of energy resources and could play a major role mitigating effects of climate change [1]. Water gas shift (WGS) reaction is one of the key steps in hydrogen production for ammonia and Fischer-Tropsch synthesis [2]. Due to recent developments in the fuel cell technology, WGS reaction is also used in the energy power generation systems for CO-free hydrogen production. WGS reaction not only mitigates CO concentration but also increases the hydrogen content of reformer stream. WGS reaction is mildly exothermic and equilibrium limited. Therefore, in industry, WGS reaction is carried in two stages, namely high temperature shift over Fe_3O_4/Cr_2O_3 at 350–500 °C and low temperature shift over $Cu/ZnO/Al_2O_3$ at 200–250 °C for high activity and CO conversion [3,4]. However, the commercially available catalysts used in two stage processes are not suitable for hydrogen production because of their cumbersome activation procedure, sensitivity to start-up/shut-down cycles and pyrophoricity [5]. It is of great interest to develop highly active, selective, cost effective, thermally stable and non pyrophoric WGS catalyst.

Ceria, as support, offers unique properties due to its oxygen storage capacity (OSC) for reactions such as three-way automotive catalysts [6], preferential CO oxidation [7], and catalytic oxidation of hydrocarbons [8,9]. The addition of noble/transition metal at low concentration alters the redox and catalytic properties of ceria based compounds [10–12]. The noble metal (Au, Pt, Rh, Pd etc.) modified CeO_2, TiO_2 and ZrO_2 are receiving widespread attention as low temperature WGS catalysts [13–17]. However, the cost of noble based catalysts makes them detrimental for large scale applications. Further, these catalysts are bifunctional whereby CO adsorbs on the metal and the dissociation of H_2O take place over ceria support [18]. The low activation energy barrier for the dissociation of H_2O and low adsorption energy of CO are the key factors for the developments of low temperature WGS catalyst [19]. Therefore, the creation of oxide ion vacancies are desirable for dissociation of H_2O molecules [20]. The substitution of aliovalent ions in the form of M^{2+}/M^{3+} not only create vacancies but also induce redox couples in the substituted metals as well as in ceria and renders strong metal support interactions.

The performances of bimetallic catalysts are often superior to those of monometallic materials [21,22]. The higher flexibility in chemical composition and interatomic arrangement compared to monometallic materials can render a new reaction pathway [23]. Previously, we have reported improvement in the activity and selectivity of bimetallic catalysts for WGS reaction [24]. Recently, it has been shown that Cu/Pt and Cu/Pd modified ceria are promising candidates for low temperature WGS reaction [25,26].

* Corresponding author. Tel.: +91 80 22932321; fax: +91 80 23601310.
E-mail address: giridhar@chemeng.iisc.ernet.in (G. Madras).

0926-3373/$ – see front matter © 2012 Elsevier B.V. All rights reserved.
http://dx.doi.org/10.1016/j.apcatb.2012.11.021

Monometallic Cu/CeO_2 and Ni/CeO_2 are also highly active and competitive for noble metal supported catalysts [27]. Further, Ni is more reactive toward H_2O than Cu in WGS reaction [28]. Therefore, the exploration of bimetallic catalyst based on Ni is desirable for the low temperature shift reaction. The improvement in the stability and activity of Ni supported catalysts is manifested on the addition of metal such as Rh, Cu, Pt, Pd, Mo and Co for reforming reactions [29,30]. However, the evaluation of the performance of such catalysts toward WGS reaction for hydrogen production has not been reported in the literature. Thus, it is of interest to investigate Pd modified Ni/CeO_2 ionic bimetallic catalyst for WGS reaction.

It is impractical for most of the polymer electrolyte membrane (PEM) fuel cells to consume all hydrogen and recycling of unused mixture of hydrogen and carbon dioxide is the usual method to make the operation economical. However, recycling of exhaust builds up the concentration of CO_2 in the system, which consequently dilutes the fuel gas leading to lower the performance of fuel cell. Therefore, it is imperative to treat the exhaust of fuel cell for removal of hydrogen. The exhaust from the PEM fuel cell can be sent to a waste hydrogen burner and heat recovery steam generator to produce steam for further utilization. Thus, direct combustion of H_2 is a common way to extract energy contained in H_2. However, catalytic hydrogen combustion (CHC) offers some advantages over direct combustion of H_2. CHC reaction can be carried out over a catalyst at lower temperatures compared to thermal oxidation and the removal of H_2 even at low concentrations is possible by catalytic oxidation [31]. The applications of CHC reactions are also prevalent in various other systems. One such application involves the prevention of destructive explosion in nuclear reactor. H_2 acts as reducing agent in various reactions such as selective catalytic reduction (SCR) of NO [32], hydrogenation of alkenes [33] etc. CHC reaction is also an integral part for the preferential oxidation (PROX) of CO in H-rich gas that used for the purification of feed gas for PEM fuel cell [34]. Detailed applications of CHC in different systems can be found in our previous study [35]. Further, the recombination of H_2-O_2 is a fundamental catalytic oxidation reaction. Therefore, the catalytic performance of the synthesized compound toward CHC reaction was also studied separately in order to understand the kinetics and mechanism of CHC reaction.

The objective of the present study is to synthesize a bifunctional, bimetallic catalyst with high activity and selectivity for WGS reaction. Therefore, Pd modified Ni/CeO_2 catalyst was synthesized by single stage solution combustion and characterized by XRD, TEM, XPS, TPR and BET surface analyzer techniques. The activity of synthesized compound toward WGS and CHC reactions was investigated and steady state kinetics measurements of both the reactions were also carried out over a wide range of temperature. The reversibility of the catalyst in the redox gas treatment is necessary for ceria mediated redox process, and, therefore, cyclic redox behavior of catalysts was also studied using H_2-TPR experiments. Mechanisms for both the WGS and CHC reactions were proposed to correlate the experimental data.

2. Experimental

2.1. Catalyst synthesis and characterization

Pd and Ni substituted CeO_2 was synthesized by a single step solution combustion method. This involves the combustion of a salt of the ceria and a Pd/Ni metal salt with a fuel in a solution. For the synthesis of $Ce_{0.88}Pd_{0.02}Ni_{0.1}O_{2-\delta}$, ceric ammonium nitrate [$(NH_4)_2Ce(NO_3)$, (Nice Chemicals, India)], palladium dichloride [$PdCl_2$ (Merck, India)], nickel nitrate [$Ni(NO_3)_2.6H_2O$ (S.D Fine Chem, India)] and urea (Fisher Scientific, India) as a fuel were taken in the molar ratio of 0.88: 0.02: 0.1: 3.7. The reactants were dissolved in 30 cm^3 water and introduced into a preheated muffle furnace at 400 °C. The solution boiled with frothing, foaming and redox mixture after dehydration, and ignited yielding a voluminous solid product within a few minutes. A similar procedure was followed for the synthesis of $Ce_{0.9}Ni_{0.1}O_{2-\delta}$. Both the combustion products were finely grounded and used for the catalytic reaction.

The catalysts were characterized by powder X-ray diffraction (XRD), transmission electron microscopy (TEM) and X-ray photoelectron spectroscopy (XPS). XRD pattern was recorded on a Phillips X'Pert diffractometer using a Cu Kα radiation source at a scan rate of 0.02 min^{-1} in the 2θ range of 10–80°. JANA 2000 program suite package was used for XRD analysis and profile refinement methodology was used to obtain the structural changes in the CeO_2 on the substitution of Pd/Ni metal ions. The electronic structure of both the catalysts before and after the reaction was determined by XPS on a Thermo Scientific Multilab 2000 system using Al Kα radiation (1486.6 eV). Binding energies of core levels of metal ions were adjusted relative to binding energy of C (1s) observed at 285 eV.

The particle size and morphology of catalyst were characterized by TEM analysis. The catalyst powder was dispersed in ethanol using an ultrasound bath and a drop of the suspension was placed on a carbon film covered copper grid (300 mesh sizes). Image and diffraction pattern were obtained on a FEI Technai 20 electron microscope operating at 200 kV. High-resolution (HRTEM) images were also obtained. The surface area of the catalysts was measured by nitrogen adsorption at 77.4 K with SMART SORB 93 model (Smart Instruments Company Pvt. Ltd, India). The catalyst samples were degassed at 150 °C for 5 h prior to the measurement.

2.2. Temperature programmed reduction (H_2-TPR)

Temperature programmed reduction (H_2-TPR) was used to study the effect of Pd and Ni metal substitution on the oxygen storage capacity (OSC) of ceria. Cyclic redox behavior or OSC of both the catalysts were also studied by H_2 -TPR or hydrogen uptake. 25 mg of the catalyst sample (50–100 mesh sizes) was plugged with ceramic wool in a quartz reactor of length 30 cm and 0.4 cm ID. The sample was first pretreated in a flow of pure Ar (Chemix, Bangalore, India) at 400 °C for 30 min in order to get a stable baseline and then, H_2-TPR experiment was performed by heating the catalyst sample from 25 to 500 °C at constant rate of 10 °C/min, in a 5% H_2/Ar gas mixture (Chemix, Bangalore, India) with total flow rate of 30 cm^3/min. The H_2-uptake during the reaction was measured using a TCD and H_2 consumption was calculated from the area under the curve which was calibrated by the quantitative reduction of known weight of CuO. Therefore, the amount of H_2 uptake or equivalent lattice release was determined.

2.3. Catalytic experiments

Catalytic experiments were conducted in a packed bed quartz reactor tube (30 cm in length and 0.4 cm of ID) operated isothermally at atmospheric pressure, in the temperature range of 60 to 500 °C. All the catalysts were used in the as-prepared form without further activation. 300 mg of catalyst in granules form (170–420 micron) was loaded in the reactor and was diluted by adding the required amount of silica granules of 150–290 micron. The reactor tube was heated from outside using an electric furnace. The temperature was measured by a K-type thermocouple placed at the center of the packed bed, and was controlled by a PID controller. The reactant gases (all supplied by Chemix Bangalore, India) were certified calibration gas mixtures with high purity (99.9%). The

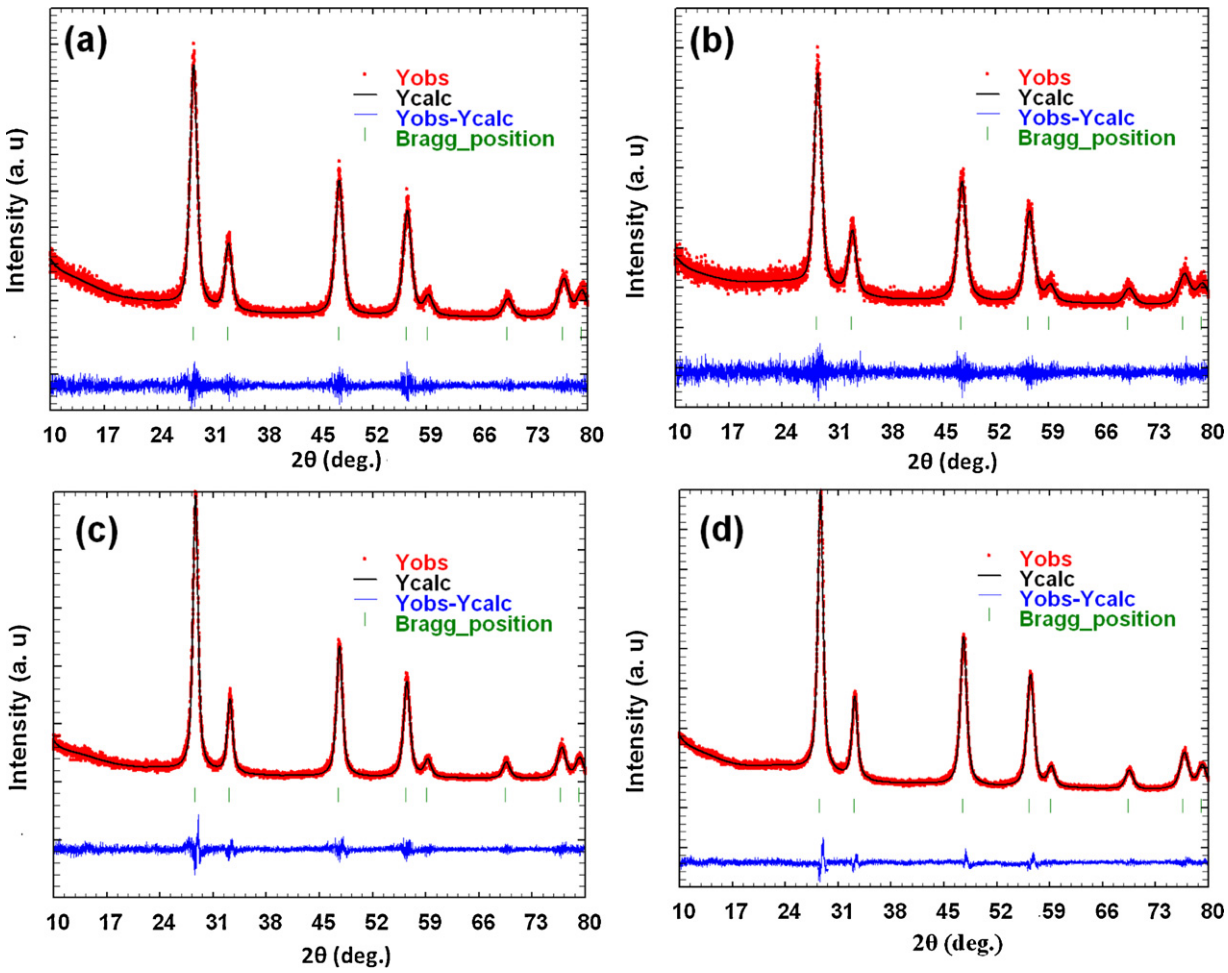

Fig. 1. Profile refined XRD patterns for $Ce_{0.9}Ni_{0.1}O_{2-\delta}$ (a) before reaction (b) after the reaction, respectively and for $Ce_{0.88}Pd_{0.02}Ni_{0.1}O_{2-\delta}$ (c) before the reaction (d) after the reaction, respectively.

reaction mixture consisted of 2 mol% of CO and balance of N_2 to keep the total gas flow rate at 100 cm^3/min. The corresponding gas hourly space velocity (GHSV) on the dry basis was 48000 h^{-1}. Water was pumped by a calibrated HPLC pump into the vaporizer maintained at 150 °C and then mixed with reactant stream line before entering the catalysts bed. A moisture trap was placed at the exit of the reactor to condense unreacted water. The feed and product gas streams were analyzed by a gas chromatograph equipped with a FID and TCD detectors. The signal of CO_2 in FID was detected by incorporating a methanizer (>99.9% efficiency) in presence of Ru catalyst operating at 350 °C. A packed column, Hayesep-A (80–100 mesh), was used to separate CO, CO_2 and CH_4 (if any) and a molecular sieve 5A column was used to separates mixture of H_2, and N_2.

Catalytic hydrogen combustion (CHC) was carried out over Pd- and Ni- modified ceria compounds. Reaction was carried out with the feed mixture consisting of 2.7 vol% of H_2, 2.7 vol% of O_2 and balance N_2 keeping the total flow rate at 100 cm^3/min. 100 mg of $Ce_{0.9}Ni_{0.1}O_{2-\delta}$ and 25 mg of $Ce_{0.88}Pd_{0.02}Ni_{0.1}O_{2-\delta}$ and $Ce_{0.98}Pd_{0.02}O_{2-\delta}$ catalysts diluted by with required amount of silica granules (50–100 mesh) was used for the CHC reaction. An increase in the weight of the catalyst beyond the mentioned amount did not increase H_2 conversion. CHC being a highly exothermic reaction; it is always desirable to use a lesser amount of catalyst in order to minimize the formation of hot spots in the catalytic bed. Therefore, the present set of reaction conditions are optimal and present a correct qualitative description for the reaction.

3. Results and discussion

3.1. Structural studies

The particle size and crystal structure of Pd and Ni modified CeO_2 were investigated using XRD and TEM analysis. XRD patterns of $Ce_{0.9}Ni_{0.1}O_{2-\delta}$ and $Ce_{0.88}Pd_{0.02}Ni_{0.1}O_{2-\delta}$ are shown in Fig. 1. All peaks in the diffraction pattern for both the sample were indexed to the fluorite structure of CeO_2 (space group Fm3 m, no 225) and the absence of peaks corresponding to Pd/Ni metal or metal oxide suggests that Pd and Ni metal ions are substituted in the ceria lattice. The changes in the structural parameters on the substitution of Pd and Ni metal were obtained by refining XRD pattern using JANA 2000 suite program. Pseudo-Voigt was used as peak shape function and Legendre polynomial (no of terms =15) was as background function and the observed XRD pattern was fitted against the calculated pattern. The symbols in Fig. 1 show the observed XRD pattern while the solid lines show the calculated XRD pattern. The difference between the observed and calculated pattern is also shown at the bottom of figure. The lattice parameters of $Ce_{0.9}Ni_{0.1}O_{2-\delta}$ and $Ce_{0.88}Pd_{0.02}Ni_{0.1}O_{2-\delta}$ are found to be 5.3931 Å and 5.3915 Å respectively. A decrease in the lattice parameter of $Ce_{0.9}Ni_{0.1}O_{2-\delta}$ and $Ce_{0.88}Pd_{0.02}Ni_{0.1}O_{2-\delta}$ compared to unsubstituted CeO_2 (5.4111 Å, JCPDS No: 340394) also confirms the substitution of smaller Ni^{2+} and Pd^{2+} ions for larger Ce^{4+} ions in the CeO_2 lattice. The observed XRD peaks are broad suggesting that the crystallites are nanometer in size. The average crystallite size was determined

Table 1
Structural parameters for the ceria modified compounds obtained by profile refinement.

Compound	Lattice Parameter (a)	R_p	R_{wp}	χ^2	Crystallite size (nm)
$Ce_{0.9}Ni_{0.1}O_{2-\delta}$ (before reaction)	5.3931	3.77	4.33	1.91	13
$Ce_{0.9}Ni_{0.1}O_{2-\delta}$ (after reaction)	5.3967	2.33	3.34	1.89	14
$Ce_{0.88}Pd_{0.02}Ni_{0.1}O_{2-\delta}$ (before reaction)	5.3915	3.88	3.53	1.57	18
$Ce_{0.88}Pd_{0.02}Ni_{0.1}O_{2-\delta}$ (after reaction)	5.3957	4.54	4.82	1.12	20

from the Scherrer formula and was found to be 13 nm and 18 nm respectively, for $Ce_{0.9}Ni_{0.1}O_{2-\delta}$ and $Ce_{0.88}Pd_{0.02}Ni_{0.1}O_{2-\delta}$. Crystallite sizes and lattice parameters, R_{wp}, R_p, and $\chi 2$ obtained from the profile refinement for both the compounds are summarized in Table 1.

The XRD patterns were also recorded after the reaction for both the catalysts to observe the changes in the crystal structure and the structure of the spent catalysts was refined, as mentioned earlier. Fig. 1(b) and (d) shows the profile refined XRD pattern of $Ce_{0.9}Ni_{0.1}O_{2-\delta}$ and $Ce_{0.88}Pd_{0.02}Ni_{0.1}O_{2-\delta}$, respectively, after the reaction. Both the patterns were indexed to fluorite structures of ceria and peaks corresponding to Pd/Ni or metal oxide metal impurities were not observed. This shows that the structure of both the catalysts remains stable after the reaction. Lattice parameters of both the spent catalysts obtained by profile refinement are given in Table 1. A slight increase in the lattice parameter as compared to as-synthesized catalyst was observed in both the spent catalysts. This indicates that both the catalysts are in partially reduced state after the reaction. This is also further supported by XPS studies.

The morphological analysis of $Ce_{0.88}Pd_{0.02}Ni_{0.1}O_{2-\delta}$ was carried out by TEM. The bright field and HRTEM images of as-synthesized $Ce_{0.88}Pd_{0.02}Ni_{0.1}O_{2-\delta}$ are shown in Fig. 2. The particle sizes are in the range of 20–25 nm, which is similar to that calculated by XRD. An isolated Pd/Ni metal particle was not observed in the bright field image and the selected area diffraction pattern (inset of Fig. 2(a)) can be indexed to fluorite structure of CeO_2. At higher magnification, a well defined lattice fringe in HRTEM image (Fig. 2(b)) confirms the crystalline nature of the sample. The widths of lattice fringes are 3.11 Å, which corresponds to d_{111} of CeO_2. EDX analysis was also carried out over the lattice fringes (111) planes and the molar ratio of Ce, Ni and Pd were found to be 0.88: 0.09: 0.03, which is close with the composition taken for the synthesis. Therefore, the combined XRD and TEM results show that Pd, Ni and CeO_2 form a complete solid solution and crystallize in the cubic fluorite structure. The BET surface area for $Ce_{0.9}Ni_{0.1}O_{2-\delta}$ and $Ce_{0.88}Pd_{0.02}Ni_{0.1}O_{2-\delta}$ was found to be 82 and 79 m^2/g, respectively.

The nature of interactions between the substituted ions and the ceria support was investigated by XPS. The oxidation states of various metal ions of $Ce_{0.9}Ni_{0.1}O_{2-\delta}$ and $Ce_{0.88}Pd_{0.02}Ni_{0.1}O_{2-\delta}$ were determined by XPS. The observations from XPS were also used for propose a reaction mechanism. The spectra were recorded both before and after the reaction. After the reaction, the flow of the reactant gases was stopped and the catalyst bed was allowed to cool to room temperature in a stream of N_2. The catalyst was quickly transferred to the vacuum chamber of the spectrometer. The sample was etched in Ar stream in order to avoid the misleading spectra of oxide species. Different spent samples of the same catalyst after different reaction runs were analyzed and reproducible results were obtained.The core level spectra of Ni (2p) before and after the reaction are shown in Figs. 3(a) and 4(b), respectively, for $Ce_{0.9}Ni_{0.1}O_{2-\delta}$ and $Ce_{0.88}Pd_{0.02}Ni_{0.1}O_{2-\delta}$. The binding energies were adjusted with respect to the binding energy of C(1s) observed at 284.5 eV. Ni ($2p_{3/2}$) binding energy is observed at 854 eV along with the broad satellite centered at around 860 eV which is characteristic of NiO species [36]. The binding energy of Ni (2p) in both the compounds is slightly higher (0.9 eV) than that of NiO, indicating that the chemical environment of the substituted Ni ions in both the compounds is different from that of the Ni ions in NiO. Ni was present in the 2+ state in both the as-synthesized compounds. After the reaction, mixture of Ni^0 and Ni^{2+} was observed in both the spent catalysts.

Further, after the reaction, the satellite peak in the XPS spectra of Ni was found to be slightly weak and shifted to higher binding

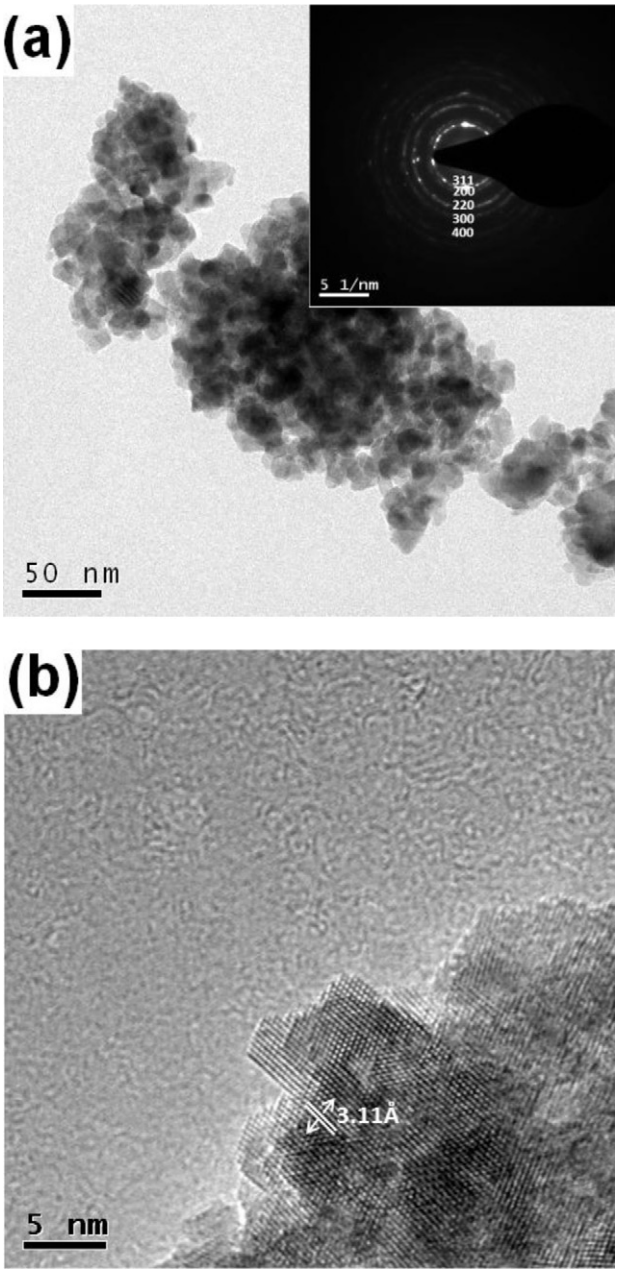

Fig. 2. (a) Bright field image and (b) HRTEM image of $Ce_{0.88}Pd_{0.02}Ni_{0.1}O_{2-\delta}$ with indexed electron diffraction in the inset of (a).

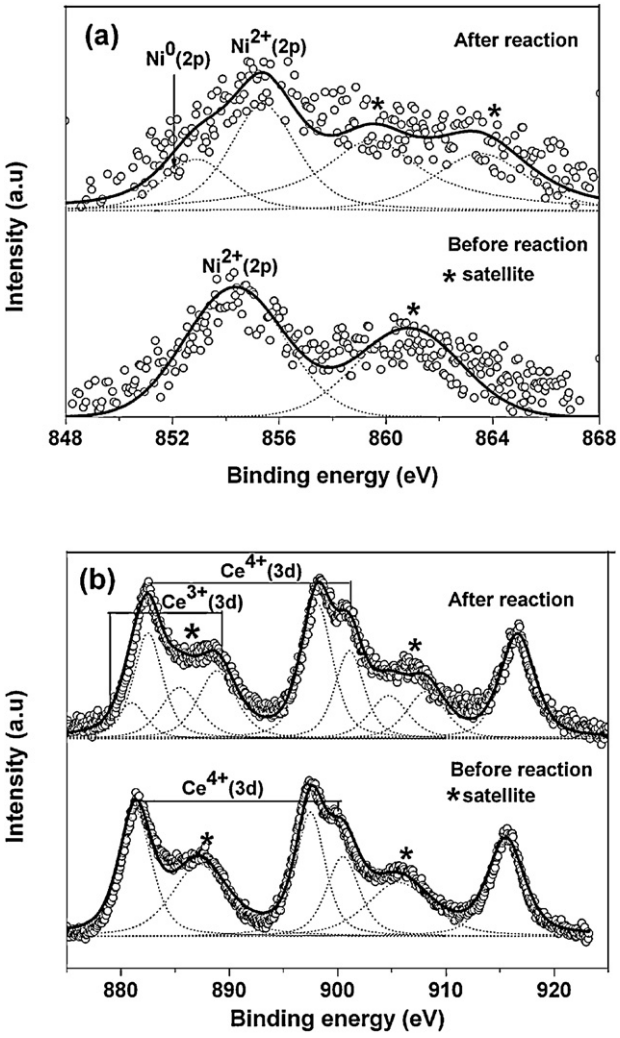

Fig. 3. Core level XPS of (a) Ni 2p and (b) Ce 3d in $Ce_{0.9}Ni_{0.1}O_{2-\delta}$.

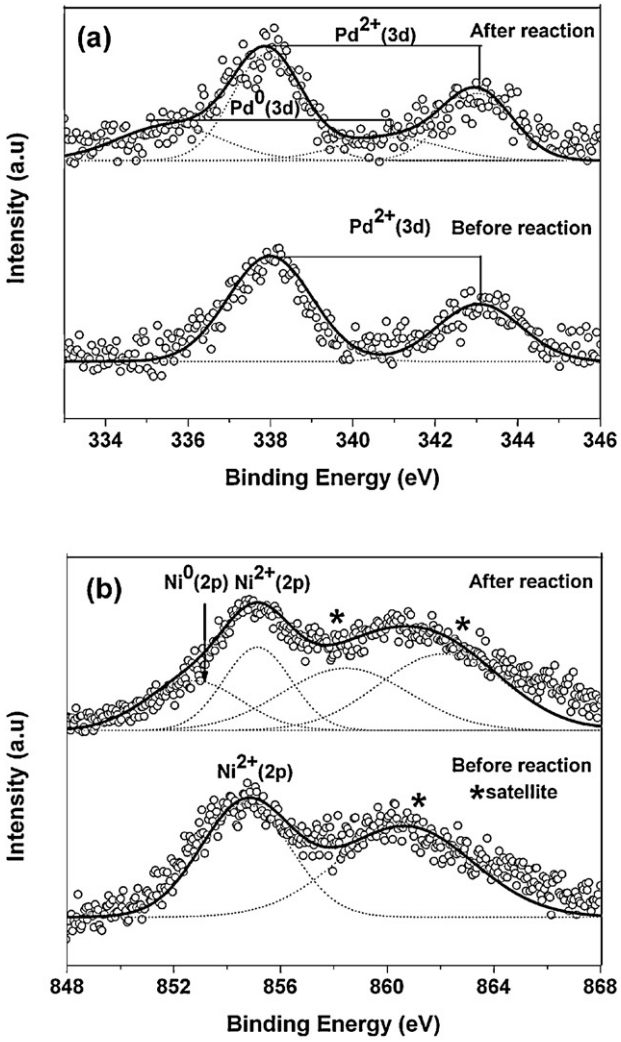

energy, indicating the formation of Ni-Pd alloy [37]. However, the OSC of the catalyst does not change in the multiple H_2-TPR cycles indicating the catalytic activity will be similar despite the formation of the alloy.

Fig. 4(a) shows the Pd (3d) spectra before and after the reaction in $Ce_{0.88}Pd_{0.02}Ni_{0.1}O_{2-\delta}$. The binding energies of Pd metal and Pd^{2+} in PdO are at 335 eV and 337.5 eV, respectively [38]. Binding energy of Pd (3d) peaks in $Ce_{0.88}Pd_{0.02}Ni_{0.1}O_{2-\delta}$ are close to the binding energy of Pd^{2+} in $PdCl_2$ and $Pd(NO_3)_2$ [39]. This indicates that Pd^{2+} ions in $Ce_{0.88}Pd_{0.02}Ni_{0.1}O_{2-\delta}$ catalyst are ionic in nature. It can be seen from Fig. 4(a) that Pd is present in 2+ oxidation state in the as-synthesized catalyst. However, the XPS spectra after the reaction showed broad peak indicating multiple oxidation states of Pd. Therefore, the main Pd (3d) peak was de-convoluted corresponding to the Pd^{2+} and Pd^0 states and the relative concentration of Pd was calculated from the intensities of main core level peak of respective cation as

$$Concentration,\ C_M = \frac{I_M/(\lambda_M \sigma_M D_M)}{\sum \left(I_M/(\lambda_M \sigma_M D_M)\right)} \quad (1)$$

Where I_M is the integral intensity of the core levels, λ_M is the mean escape depths of the respective photoelectrons, σ_M is the photoionization cross section, and D_M is the geometric factor. The value for photoionization cross-section and mean escape depths were taken from the literature [40,41]. The relative concentration

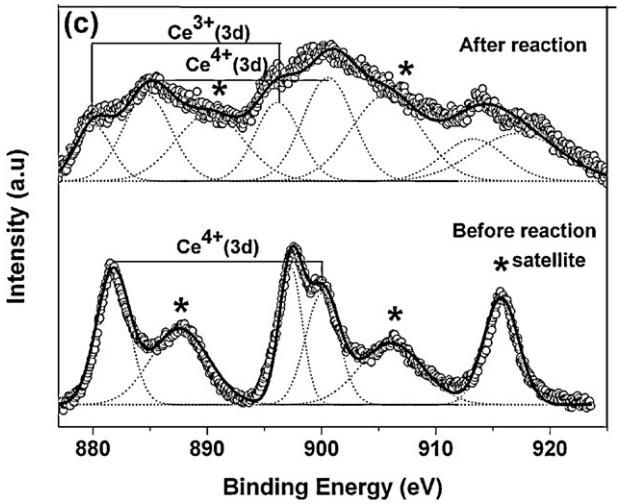

Fig. 4. Core level XPS of (a) Pd (3d) (b) Ni 2p and (c) Ce 3d in $Ce_{0.88}Pd_{0.02}Ni_{0.1}O_{2-\delta}$.

of the Pd^0 and Pd^{2+} was calculated from deconvoluted peaks and found to be to be 33% and 67% (±3% error), respectively for Pd^0 and Pd^{2+} states.Figs. 3(b) and 4(c) show the XPS of Ce (3d) in the both the catalysts before and after the reaction. The core level spectra of Ce (3d) are complex and 10 peaks were fitted: 3 doublets for CeO_2

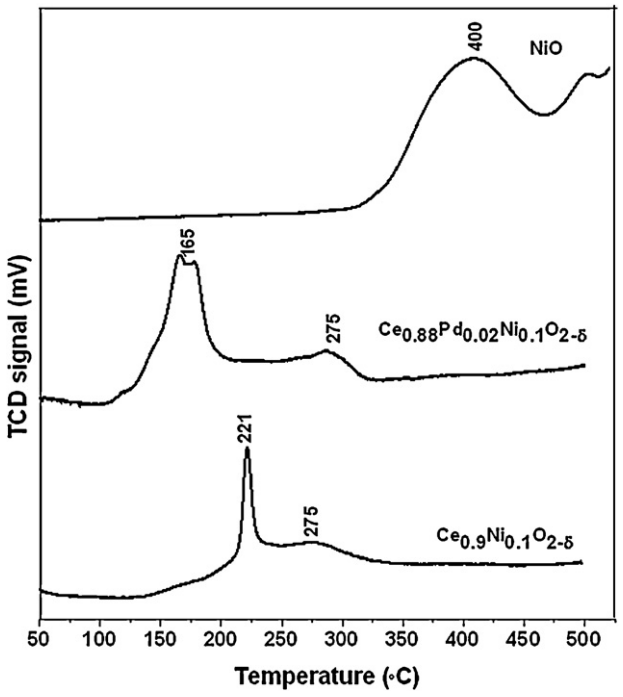

Fig. 5. H_2-TPR profile for ceria modified compounds and nickel oxide.

and 2 for Ce_2O_3 [42]. The presence of Ce ($3d_{5/2}$) peak at 882.7 eV and satellite peaks at 889.1 eV correspond to Ce in the 4+ state in both the as-synthesized sample. After the reaction, a partial filling of the valley between Ce^{4+} ($3d_{5/2}$) at 882.7 eV and its satellite at 889.1 eV was observed. The Ce 3d spectra of the both the samples denotes a mixture of mixed Ce^{3+}/Ce^{4+} oxidation states indicating that the surface of the samples is partially reduced during the reaction. The deconvolution procedure was applied to calculate the concentration of Ce^{3+} state and found to be about 8% and 17% for $Ce_{0.9}Ni_{0.1}O_{2-\delta}$ and $Ce_{0.88}Pd_{0.02}Ni_{0.1}O_{2-\delta}$, respectively. This shows that the addition of Pd in $Ce_{0.9}Ni_{0.1}O_{2-\delta}$ felicitates the reduction of Ce ions. The reduction of Ce^{4+} to Ce^{3+} during the reaction clearly shows the involvement of $Ce^{4+} \leftrightarrow Ce^{3+}$ redox couple during the reaction. It indicates that the utilization of lattice oxygen occurs during the reaction resulting in a reduction of Ce^{4+} to Ce^{3+}.

In addition to this, the XPS studies show strong a metal support interaction occurs during the reaction. In the as-synthesized catalysts, Ce was observed in 4+ state. The aliovalent substitution of metals (Ni/Pd) in the ceria creates oxide ion vacancies in order to maintain the electrostatic neutrality of the crystal and these oxygen deficient sites act as sites for the dissociative adsorption of H_2O molecules. In this way, the oxide ion vacancies facilitate the dissociation of H_2O during the reaction.

3.2. H_2-TPR experiments

The redox property and the high lattice oxygen mobility of ceria are the most important factors that govern the catalytic activity of CeO_2 in WGS reaction. Therefore, H_2-TPR was used to characterize the reducibility of ceria modified compounds. The H_2-TPR profiles of ceria based compounds are shown in Fig. 5. H_2-TPR of the pure NiO sample was also included for the comparison showing a broad reduction peak centered at 400 °C. The addition of Ni and Pd has no effect on the bulk reduction of ceria. Therefore, only H_2 consumption at low temperatures was determined. The addition of Ni ions facilitates the reduction of CeO_2 at much lower temperature. H_2 consumption for $Ce_{0.9}Ni_{0.1}O_{2-\delta}$ was observed in the range between 150 and 300 °C. A sharp peak at 221 °C can be assigned to the reduction of Ni^{2+} species interacting with support and another small broad peak centered at 380 °C can be related to the partial reduction of ceria [43,44]. The reduction temperature of Ni^{2+} ion to Ni^0 in $Ce_{0.9}Ni_{0.1}O_{2-\delta}$ is much lower than in the pure NiO sample, indicating the reduction of Ni^{2+} ion is much easier in CeO_2 environment. The addition of Pd ion lowered the reduction temperature of $Ce_{0.9}Ni_{0.1}O_{2-\delta}$ from 221 to 165 °C. The reducibility of $Ce_{0.88}Pd_{0.02}Ni_{0.1}O_{2-\delta}$ at much lower temperature as compared to $Ce_{0.9}Ni_{0.1}O_{2-\delta}$ exhibits strong metal support interactions. The combined results of TPR and XPS studies show the enhancement in catalytic activity of $Ce_{0.88}Pd_{0.02}Ni_{0.1}O_{2-\delta}$ in comparison with $Ce_{0.9}Ni_{0.1}O_{2-\delta}$ and can be attributed to the higher oxygen mobility via a redox cycle. Therefore, the increase in the WGS activity for $Ce_{0.88}Pd_{0.02}Ni_{0.1}O_{2-\delta}$ is mainly through the participation of the lattice oxygen at low temperature, which is subsequently rejuvenated by oxygen from water molecule.

3.3. Cyclic redox behavior

The reversibility of catalyst in the redox gas treatment is important for long term catalytic activity and sustainability. Therefore, cyclic redox behavior of both the catalysts was studied by H_2-TPR experiment. The catalyst after first H_2-TPR cycle (C_1) was cooled to 300 °C in pure Ar, and then reoxidized in air at 300 °C for 30 min. After the reoxidation, the catalyst was allowed to cool to room temperature (25 °C) in pure Ar and the second H_2-TPR cycle (C_2) was repeated. Three consecutive redox cycles were performed. The area under the H_2-TPR curve was used to calculate the oxygen storage capacity (OSC). The OSC corresponding to the three successive cycles are shown by histogram in Fig. 6. OSC up to 300 °C for the first, second and third cycle is 990, 916 and 796 μmol/g, respectively, for $Ce_{0.9}Ni_{0.1}O_{2-\delta}$ and 992, 988 and 970 μmol/g, respectively, for $Ce_{0.88}Pd_{0.02}Ni_{0.1}O_{2-\delta}$. Some loss of oxygen in subsequent cycles was observed after the first H_2-TPR cycle indicating some irreversible surface change. However, reasonably good reversibility in OSC was observed for both the catalysts. We have also previously reported similar cyclic redox behavior for ceria modified with base metals [24]. On the addition of Pd, no significant increase in the OSC of $Ce_{0.9}Ni_{0.1}O_{2-\delta}$ was observed. However, the presence of Pd shifts the surface reduction peak of $Ce_{0.9}Ni_{0.1}O_{2-\delta}$ to a lower temperature and this is the primary reason for the enhancement in the activity of $Ce_{0.88}Pd_{0.02}Ni_{0.1}O_{2-\delta}$ toward the WGS reaction.

3.4. Kinetic study of WGS

The catalytic activity of both the samples for WGS reaction was expressed as the percentage of CO conversion, in the range of 140–500 °C. Fig. 7 shows the variation of CO conversion with temperature over ceria modified catalysts. There is no decrease in CO conversion up to 500 °C over both $Ce_{0.9}Ni_{0.1}O_{2-\delta}$ and $Ce_{0.88}Pd_{0.02}Ni_{0.1}O_{2-\delta}$. The concentrations shown in Fig. 7 were normalized by the initial concentration of CO. Nearly complete (~99%) conversion of CO was achieved at 300 °C with $Ce_{0.88}Pd_{0.02}Ni_{0.1}O_{2-\delta}$ and at 380 °C with $Ce_{0.9}Ni_{0.1}O_{2-\delta}$ catalyst. $Ce_{0.9}Ni_{0.1}O_{2-\delta}$ is also a good WGS catalyst but it shows activity at a higher temperature. The undesirable products from possible side reaction such as CH_4 and other hydrocarbons were not detected in the outlet stream within the detection limit of 5 ppm and CO conversion is almost 99% indicating high selectivity of both the catalysts toward H_2 production. It is well reported that bulk Ni species promotes the formation of CH_4 under typical WGS reaction conditions [45] and the metallic nickel is a known catalyst for methanation and Fischer-Tropsch process [46]. However, this study reports a lack of CO methanation activity over both the nickel based ionic catalysts and this may be attributed to the ionic substitution of nickel and presence of

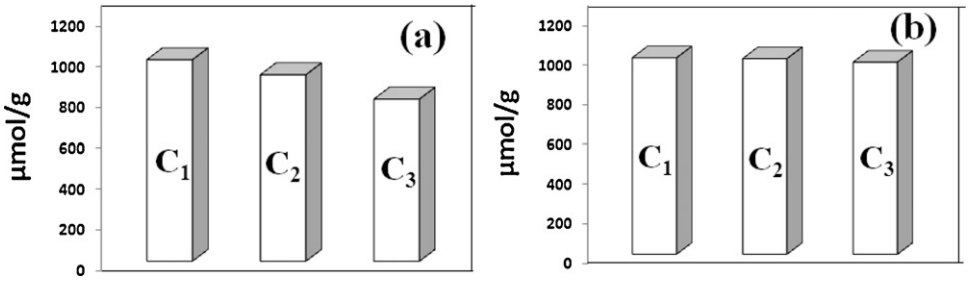

Fig. 6. OSC of (a) $Ce_{0.9}Ni_{0.1}O_{2-\delta}$ and (b) $Ce_{0.88}Pd_{0.02}Ni_{0.1}O_{2-\delta}$ after three consecutive reduction cycles.

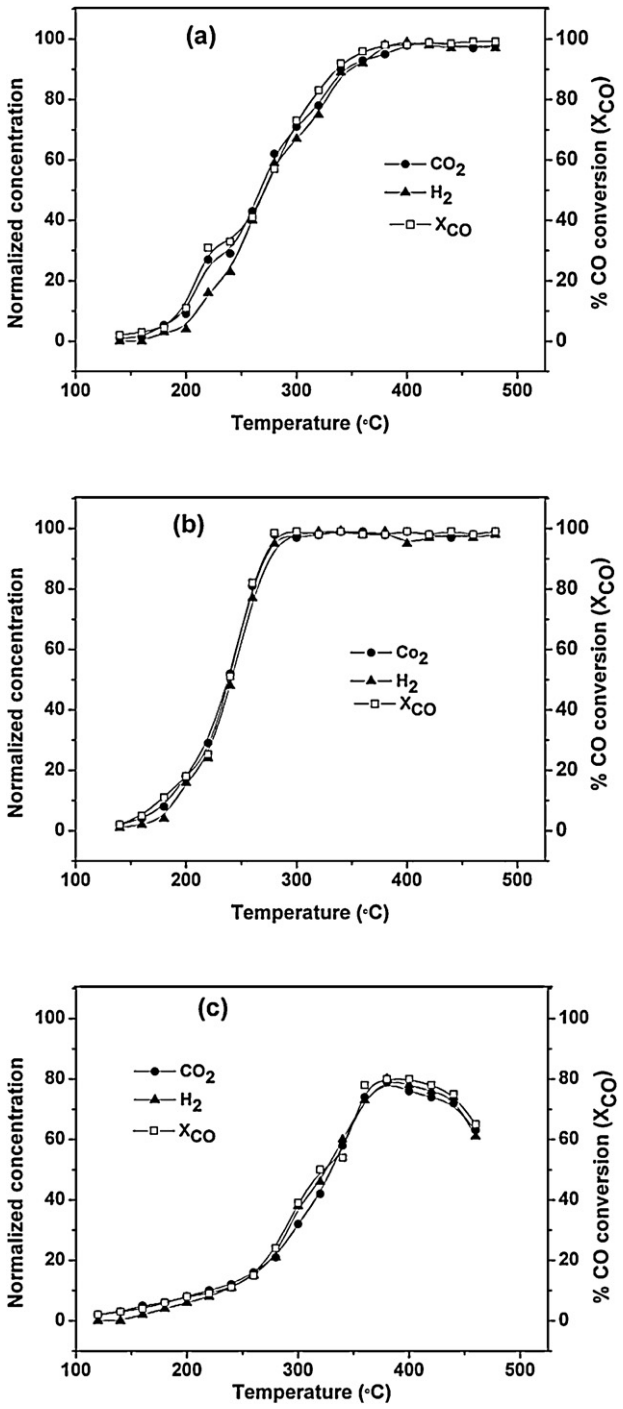

Fig. 7. Normalized CO, CO_2 and H_2 concentrations in WGS reaction over (a) $Ce_{0.9}Ni_{0.1}O_{2-\delta}$ (b) $Ce_{0.88}Pd_{0.02}Ni_{0.1}O_{2-\delta}$ and (c) $Ce_{0.98}Pd_{0.02}O_{2-\delta}$.

excess H_2O vapor. The present finding is also consistent with the literature and either suppression or no detection of CH_4 activity is reported over Ni modified ceria catalyst [47–49]. Recently, it has been reported that the addition of basic oxides to Pt and Pd catalysts help suppress formation of CH_4 [50].

The WGS reaction was also carried out over 300 mg of 2 at% Pd substituted CeO_2 ($Ce_{0.98}Pd_{0.02}O_{2-\delta}$) synthesized by a solution combustion method and the activity of this compound was compared with those of $Ce_{0.9}Ni_{0.1}O_{2-\delta}$ and $Ce_{0.88}Pd_{0.02}Ni_{0.1}O_{2-\delta}$ catalysts. The feed consisting of 2 vol% of CO and 98% of N_2 with the total gas flow rate 100 cm^3/min was used. Only 80% conversion of CO to CO_2 was observed around 380 °C for $Ce_{0.98}Pd_{0.02}O_{2-\delta}$ (Fig. 7(c)). The reverse WGS reaction dominates above this temperature. This clearly shows that the addition of Ni to Pt/CeO_2 enhances the activity of $Ce_{0.88}Pd_{0.02}Ni_{0.1}O_{2-\delta}$ toward WGS reaction and increase in the activity can be attributed to the increase in the amount of surface oxygen in CeO_2.

The rate of reaction and activation energy was calculated by varying the weights of the catalyst keeping the total gas flow rate constant. The reaction rates were obtained for both the catalysts in the kinetic regime and the variation of W/F_{CO} with the fractional conversion of CO is shown in Fig. 8 (a) and (b) respectively, for $Ce_{0.9}Ni_{0.1}O_{2-\delta}$ and $Ce_{0.88}Pd_{0.02}Ni_{0.1}O_{2-\delta}$. The rates of reaction over these catalysts at various temperatures were calculated from the slope of linear portion of the curve. The following equation was used to calculate rate of reaction.

$$Rate(r) = \frac{F_{CO} \times x}{W} = \frac{x}{W/F_{CO}} \quad (2)$$

where F_{CO} is the gas flow rate in mol/s, W is the weight of the catalyst in g and x is the fractional CO conversion. The variation of the rate of reaction with temperature is shown in Fig. 8(c) and (d) respectively, for $Ce_{0.9}Ni_{0.1}O_{2-\delta}$ and $Ce_{0.88}Pd_{0.02}Ni_{0.1}O_{2-\delta}$. As expected, the rate of reaction over $Ce_{0.88}Pd_{0.02}Ni_{0.1}O_{2-\delta}$ was found to be high at low temperatures compared to $Ce_{0.9}Ni_{0.1}O_{2-\delta}$ catalyst. The enhancement in the WGS activity for $Ce_{0.88}Pd_{0.02}Ni_{0.1}O_{2-\delta}$ is mainly through the participation of the lattice oxygen at low temperature as compared to $Ce_{0.9}Ni_{0.1}O_{2-\delta}$ as evident from H_2-TPR experiments. The Arrhenius equation was used to calculate activation energies for both the catalysts and the corresponding plots are given in the inset of Fig. 8(c) and (d) respectively for $Ce_{0.9}Ni_{0.1}O_{2-\delta}$ and $Ce_{0.88}Pd_{0.02}Ni_{0.1}O_{2-\delta}$. The activation energies for the reaction over $Ce_{0.9}Ni_{0.1}O_{2-\delta}$ and $Ce_{0.88}Pd_{0.02}Ni_{0.1}O_{2-\delta}$ were found to be 67 and 53 kJ/mol, respectively.

After reporting high activity of $Ce_{0.88}Pd_{0.02}Ni_{0.1}O_{2-\delta}$ catalyst in WGS reaction in the absence of feed of CO_2 and H_2, the performance of this catalyst was also examined in the presence of excess CO_2 and H_2. Therefore, WGS reaction was carried with a gas mixture consisting of 2% of CO, 10% of CO_2 and 10% of H_2 (all in vol%) and balance N_2, keeping the total gas flow at 100 cm^3/min with 300 mg of catalyst. Fig. 9 shows the normalized concentration of CO, H_2 and CO_2 as a function of temperature and the dotted line in figure depicts the equilibrium CO conversion. H_2 and CO_2

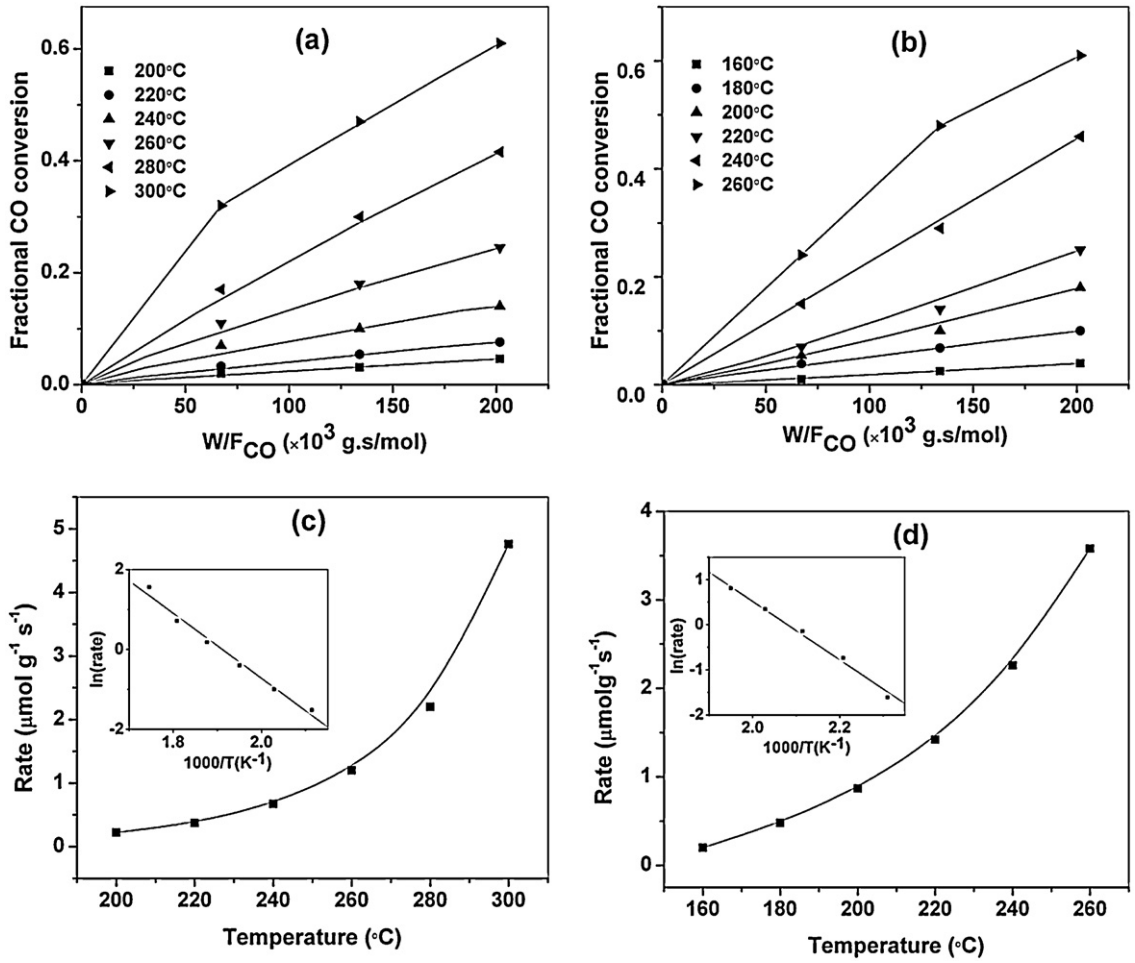

Fig. 8. Variation of fractional conversion of CO with W/F_{CO} for (a) $Ce_{0.9}Ni_{0.1}O_{2-\delta}$ (b) $Ce_{0.88}Pd_{0.02}Ni_{0.1}O_{2-\delta}$ and rate of reaction as function of temperature for (c) $Ce_{0.9}Ni_{0.1}O_{2-\delta}$ (d) $Ce_{0.88}Pd_{0.02}Ni_{0.1}O_{2-\delta}$.

concentrations are plotted by deducting the initial concentration of H_2 and CO_2. Therefore, the initial concentration of H_2 and CO_2 is zero. Nearly equilibrium conversion (~ 96%) of CO was observed at 480 °C even in the presence of feed H_2 and CO_2. The lack of CO_2 methanation activity also indicates high selectivity of this catalyst toward H_2 production. Therefore, the present catalyst is highly active and selective even in the presence of fed H_2 and CO_2.

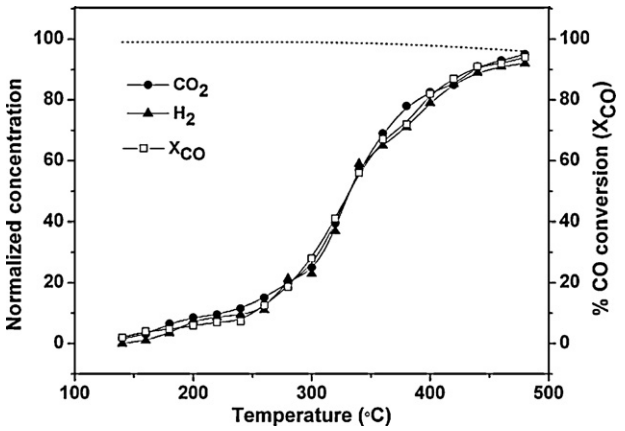

Fig. 9. Normalized CO, CO_2 and H_2 concentrations in WGS reaction over the $Ce_{0.88}Pd_{0.02}Ni_{0.1}O_{2-\delta}$ catalyst. (Feed gas composition: 2 cm^3/min of CO, 10 cm^3/min of CO_2, 10 cm^3/min of H_2 and balance N_2 to keep total flow 100 cm^3/min). Dotted line represents equilibrium CO conversion.

3.5. Kinetic study of CHC

Fig. 10 shows the variation of percentage H_2 conversion with temperature. As expected, Pd modified Ni/CeO_2 showed higher activity than $Ce_{0.9}Ni_{0.1}O_{2-\delta}$. At low temperature, $Ce_{0.88}Pd_{0.02}Ni_{0.1}O_{2-\delta}$ catalyst showed slightly higher activity

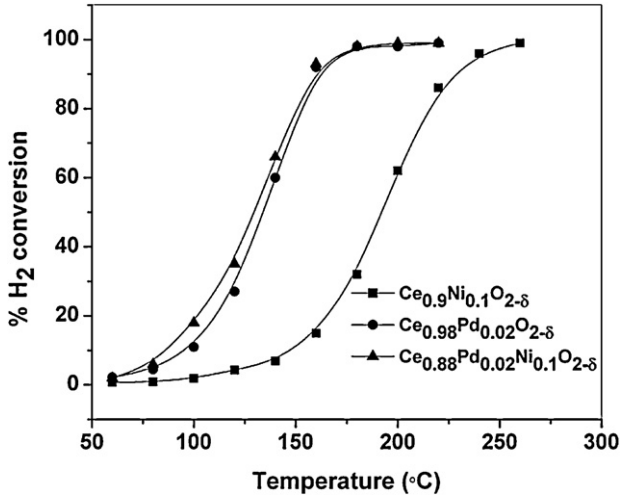

Fig. 10. Variation of H_2 conversion with temperature for CHC reaction.

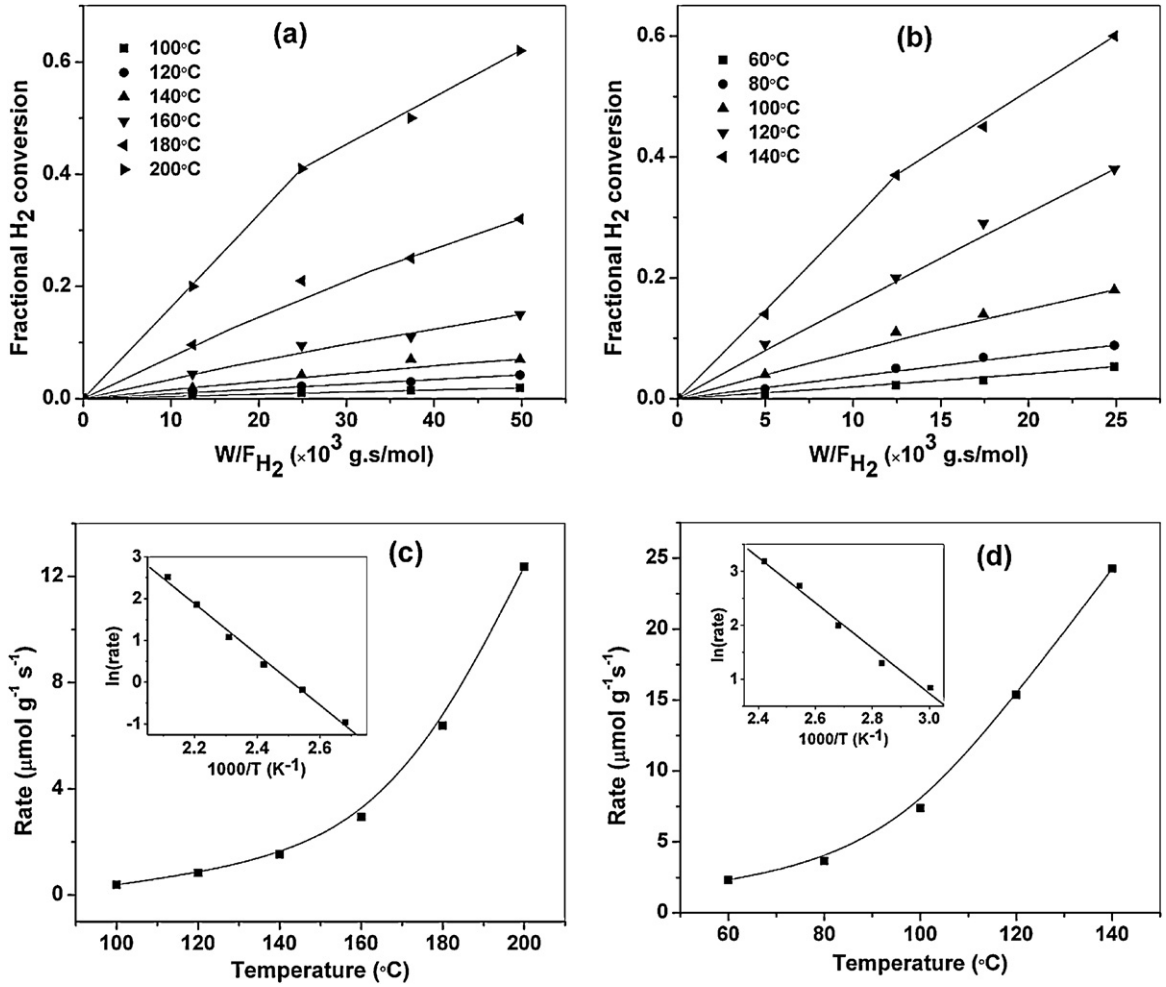

Fig. 11. Variation of fractional conversion of H_2 with W/F for (a) $Ce_{0.9}Ni_{0.1}O_{2-\delta}$ (b) $Ce_{0.88}Pd_{0.02}Ni_{0.1}O_{2-\delta}$ and rate of reaction as function of temperature for (c) $Ce_{0.9}Ni_{0.1}O_{2-\delta}$ (d) $Ce_{0.88}Pd_{0.02}Ni_{0.1}O_{2-\delta}$.

compared to $Ce_{0.98}Pd_{0.02}O_{2-\delta}$. However, both the catalysts exhibit nearly similar activity at high temperature. Experiments were also performed with different weights of the catalyst keeping the total gas flow at 100 cm^3/min. Fig. 11(a) and (b) show the variation of W/F with the fractional conversion (x) for $Ce_{0.9}Ni_{0.1}O_{2-\delta}$ and $Ce_{0.88}Pd_{0.02}Ni_{0.1}O_{2-\delta}$, respectively. The reaction rates were calculated from the slope of W/F and conversion plot and variation of rate of reaction with temperature are shown in Fig. 11 (c) and (d) for $Ce_{0.9}Ni_{0.1}O_{2-\delta}$ and $Ce_{0.88}Pd_{0.02}Ni_{0.1}O_{2-\delta}$, respectively. The activation energies for the catalysts were calculated from Arrhenius plot (inset of Fig. 11(c) and (d)) and was found to be 49 and 34 kJ/mol for $Ce_{0.9}Ni_{0.1}O_{2-\delta}$ and $Ce_{0.88}Pd_{0.02}Ni_{0.1}O_{2-\delta}$, respectively.

3.6. Kinetic models

3.6.1. WGS reaction

Much information has been published in the literature and the mechanism of WGS reaction remains controversial. Two completely different mechanisms namely, "redox mechanism" and "formate mechanism" have been proposed to describe the reaction kinetics. The redox mechanism involves the reduction of catalyst by CO followed by the reoxidation by H_2O [27,51,52]. The dopants are used to facilitate the reduction of support by increasing the utilization of lattice oxygen during the reaction. It was shown that there is indeed a relation between the WGS activity and the surface concentration of CO on the noble metals [53]. In contrast, the formate mechanism proceeds via a formate intermediate formed by the reaction between adsorbed CO with the terminal hydroxyl groups of the support [54,55]. It is important to note that these two reaction mechanisms are strongly dependent on the experimental conditions [15].

Recently, a novel steady-state isotopic transient kinetic analysis (SSTIKA) experiment coupled with mass spectrometry (MS) and DRIFTS techniques was designed to investigate the WGS reaction over Pt/CeO_2 and Pt/TiO_2. The results of this study showed a switch from the "redox mechanism" to a combination of redox and "formate mechanism" in the range of 473 to 573 K for Pt/CeO_2 and contribution from the formate mechanism to the overall WGS reaction rate was negligible. In addition to this, only redox mechanism was operative for Pt/TiO_2 [51]. In another SSITKA-DRIFTS experiment, the formation of surface formate and carbonate were observed over TiO_2 under WGS reaction conditions and this was proposed to be inactive (spectator) for the steady state WGS reaction [56]. The in-situ WGS reaction was performed over 0.5 wt.% Pt/γ-Al_2O_3 catalyst and at least two kinds of formate (–COOH) species were present on the Al_2O_3 surface, one of which was active leading to the formation of CO_2 and H_2, while the other kind was considered as the spectator [57]. For the WGS reaction over Pt/CeO_2 it has been shown that the formate is an inactive species and does not participate in the reaction [52,58]. Recently, a novel experimental methodology, in combination with transient infrared spectroscopic and isotopic studies was developed to discriminate

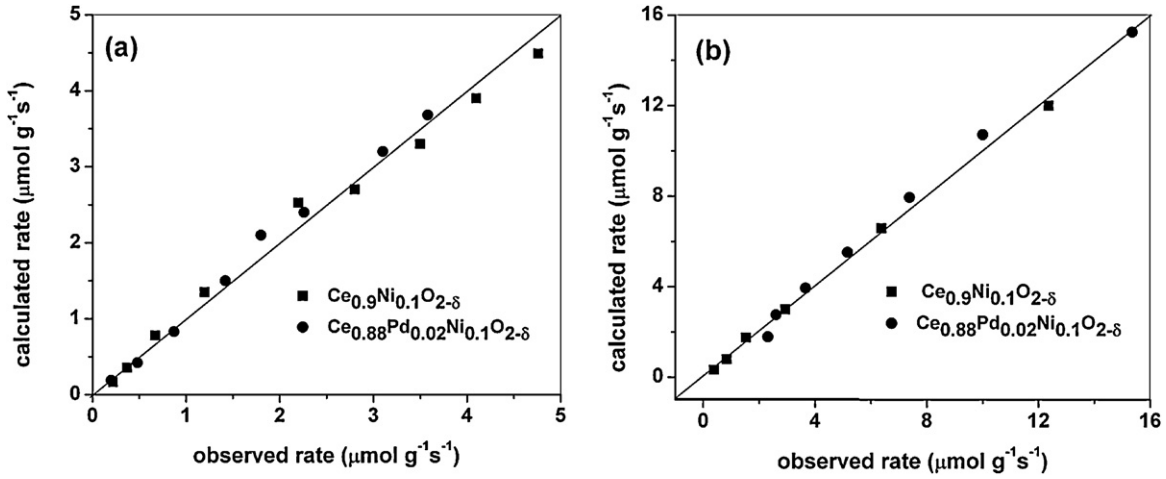

Fig. 12. Comparison between experimentally measured rate and calculated rate from the model for (a) WGS reaction and (b) CHC reaction.

the "redox" and "associative formate mechanisms" for WGS reaction over Pt/CeO_2 and showed that the formate is a less important intermediate in reaction [59].Based on the H2-TPR studies, the present study indicates that there is a direct relation between extent of ceria reducibility and WGS activity. An increase in the reducibility of ceria increases the density of active sites (i.e., vacancies in this case). Therefore, the possibility of a redox mechanism is most likely. Further, the surface formates have limited thermal stability and if formate mechanism was operative, we would expect a maximum in reaction rate at relatively low temperatures. However, Fig. 7 clearly shows that WGS rates increase steadily with increasing temperature. Therefore, based on the above discussion, the most plausible mechanism seems to be essentially a redox mechanism.

Metal oxide supported noble metal catalysts are bifunctional in nature [60]. For example, in case of Pd/CeO_2 catalyst, the adsorbed CO on the Pd reduces CeO_2 near the Pd interface and subsequently reduced CeO_2 is re-oxidized by H_2O. We have previously developed a redox mechanism for ceria modified catalysts [24]. The following mechanistic steps were assumed while deriving the rate expression and a detailed discussion on this can be found elsewhere [61].

$$CO + M \overset{K_1}{\longleftrightarrow} CO_M \tag{3}$$

$$CO_M + Ce^{4+} \xrightarrow{k_2} CO_2 + Ce^{3+\square} \tag{4}$$

$$H_2O + Ce^{3+\square} \xrightarrow{k_3} H_2 + Ce^{4+} \tag{5}$$

M and $Ce^{3+\square}$ represents metal (Pd or Ni) and oxide vacancy, respectively. In brief, equation (3) depicts the reversible adsorption of CO over the metal ion. The adsorbed CO extracts lattice oxygen from ceria surface to form CO_2 creating oxide vacancy and H_2O rejuvenates this oxide vacancy for the completion of the redox cycle. The following rate expression was used to fit the experimental data for both the catalysts.

$$r_{farward} = \frac{K_1 k_2 k_3 C_{CO} C_{H_2O}}{K_1 k_2 C_{CO} + k_3 C_{H_2O}(1 + K_1 C_{CO})} \tag{6}$$

3.6.2. CHC reaction

On the basis of above discussion, it can be deduced that both the compounds are reducible and utilization of lattice oxygen is indeed possible during the reaction. Therefore, a similar analogy is used to propose reaction mechanism for CHC reaction and the plausible reaction steps for CHC are represented as

$$H_2 + 2M \overset{K_4}{\longleftrightarrow} 2H - M \tag{7}$$

$$O_2 + 2V \overset{K_5}{\longleftrightarrow} 2"O" \tag{8}$$

$$"O" + H - M \xrightarrow{k_6} "O"H + M \tag{9}$$

$$"O"H + H - M \xrightarrow{k_7} H_2O + M + V \tag{10}$$

M, V, "O" refer to the vacant sites on support (Ni or Pd cations), oxide ion vacancy on support and adsorbed oxygen species on the support, respectively. Equation (7) represents the dissociative adsorption of H_2 over metal cations. As mentioned earlier, the ionic substitution of aliovalent ions not only creates oxide ion vacancies but also improve oxygen mobility. It is also known that these vacancies are the best sites for oxygen adsorption/dissociation and this phenomenon is well reported for CO oxidation and WGS reaction [62,63]. Therefore, the replenishment of lattice ion vacancies is a common step for both the WGS and CHC reaction. The adsorption of O_2 over oxide ion vacancies is depicted by equation (8). The dissociated H atoms react with the adsorbed O_2 species and gives H_2O in two steps (equations (9) and (10)) through the formation of the hydroxyl group. The formation of hydroxyl groups during H_2 chemisorption over CeO_2 has been formulated with the help of IR studies [64]. Recently, we have also developed the support dependent reaction mechanisms for CHC reaction utilizing the hydroxyl groups [35]. Based on the above elementary steps, the rate of formation of H_2O can be obtained as

$$r_{H_2O} = \frac{K_4 K_5 k_{67} C_{H_2} C_{O_2}}{\left(1 + K_5 C_{O_2}\right)\left(1 + \sqrt{K_4 C_{H_2}}\right)^2} \tag{11}$$

3.7. Model validation and Parameters estimation

A nonlinear least square optimization technique based on the Levenberg–Marquardt algorithm was used to fit the experimental data with model equations for both the reactions. The CO equilibrium constants (K_1) for Pd and Ni were taken from the literature [61,65]. The estimated rate parameters have physical relevance, and therefore, appropriate constraints were imposed while optimizing rate parameters. A model fits yielding positive activation energy and negative frequency factor were excluded from further model discrimination. Confidence limits of 95% for kinetic parameters were also estimated and the optimized rate parameters for both the reactions and catalysts are given in Table 2. The goodness of the fit is can be observed from the plots shown in Fig. 12 (a) and (b) respectively, for WGS and CHC reactions.

Table 2
Rate parameters used in the models for both WGS and CHC reactions.

Parameter	$Ce_{0.9}Ni_{0.1}O_{2-\delta}$	$Ce_{0.88}Pd_{0.02}Ni_{0.1}O_{2-\delta}$
K_1	8.5×10^{15} exp(136875/T)	1×10^{15} exp(145574/T)
k_2	0.9 exp(−6760/T)	1.9 exp(−6403/T)
k_3	1.1 exp(−8987/T)	2.2 exp(−6868/T)
K_4	5.8 exp(7176/T)	3.9 exp(6015/T)
K_5	5.7 exp(−5854/T)	6 exp(−4564/T)
k_{67}	12 exp(−5943/T)	31exp(−4554/T)

4. Conclusions

Pd modified Ni/CeO_2 synthesized by a single step solution combustion method was used for the WGS reaction. The catalyst is highly active and selective toward H_2 production and exhibits a lack of CO methanation activity. The present catalyst is reversible in cyclic redox treatment and therefore potential candidates for hydrogen production. The intimate contact between Pd, Ni and ceria support facilitates the reducibility at much low temperatures and this modification in the reducibility of the support is proposed to be the primary reason for the enhancement in the activity WGS reaction. However, no significant increase in the oxygen storage capacity was observed on the addition of Pd into Ni/CeO_2. Despite this Pd modified catalysts showed higher activity. The applicability of present catalysts was also explored to the exhaust purification for combustible gases from fuel cell processors and both the compounds showed high activity for the catalytic combustion of H_2.

Acknowledgment

Authors gratefully acknowledge the Department of Science and Technology, Government of India for financial assistance.

References

[1] J. Gómez, J. Fierro, Applied Catalysis A: General 144 (1996) 7–57.
[2] J.N. Armor, Applied Catalysis A: General 176 (1999) 159–176.
[3] C.A. Franchini, A.M. Duarte de Farias, E.M. Albuquerque, R. dos Santos, M.A. Fraga, Applied Catalysis B: Environmental 117–118 (2012) 302–309.
[4] C. Ratnasamy, J.P. Wagner, Catalysis Reviews Science and Engineering 51 (2009) 325–440.
[5] R. Gorte, S. Zhao, Catalysis Today 104 (2005) 18–24.
[6] S.Y. Christou, S. García-Rodríguez, J.L.G. Fierro, A.M. Efstathiou, Applied Catalysis B: Environmental 111–112 (2011) 233–245.
[7] M. Kipnis, E. Volnina, Applied Catalysis B: Environmental 103 (2011) 39–47.
[8] A.D. Mayernick, M.J. Janik, Journal of Physical Chemistry C 112 (2008) 14955–14964.
[9] S. Scirè, L.F. Liotta, Applied Catalysis B: Environmental 125 (2012) 222–246.
[10] I. Valsamakis, M. Flytzani-Stephanopoulos, Applied Catalysis B: Environmental 106 (2011) 255–263.
[11] H. Borchert, Y. Borchert, V.V. Kaichev, I.P. Prosvirin, G.M. Alikina, A.I. Lukashevich, V.I. Zaikovskii, E.M. Moroz, E.A. Paukshtis, V.I. Bukhtiyarov, Journal of Physical Chemistry B 109 (2005) 20077–20086.
[12] P.S. Lambrou, P.G. Savva, J.L.G. Fierro, A.M. Efstathiou, Applied Catalysis B: Environmental 76 (2007) 375–385.
[13] Y. Wang, Y. Zhai, D. Pierre, M. Flytzani-Stephanopoulos, Applied Catalysis B: Environmental 127 (2012) 342–350.
[14] I. González, R. Navarro, W. Wen, N. Marinkovic, J. Rodriguez, F. Rosa, J. Fierro, Catalysis Today 149 (2010) 372–379.
[15] R. Burch, Physical Chemistry Chemical Physics 8 (2006) 5483–5500.
[16] T. Tabakova, M. Manzoli, D. Paneva, F. Boccuzzi, V. Idakiev, I. Mitov, Applied Catalysis B: Environmental 101 (2011) 266–274.
[17] W. Deng, C. Carpenter, N. Yi, M. Flytzani-Stephanopoulos, Topics in Catalysis 44 (2007) 199–208.
[18] K. Azzam, I. Babich, K. Seshan, L. Lefferts, Journal of Catalysis 251 (2007) 163–171.
[19] C.D. Zeinalipour-Yazdi, A.M. Efstathiou, Journal of Physical Chemistry C 112 (2008) 19030–19039.
[20] R. Si, J. Raitano, N. Yi, L. Zhang, S.W. Chan, M. Flytzani-Stephanopoulos, Catalysis Today 180 (2012) 68–80.
[21] L.Y. Gan, Y.X. Zhang, Y.J. Zhao, Journal of Physical Chemistry C 114 (2009) 996–1003.
[22] W. Xu, R. Si, S.D. Senanayake, J. Llorca, H. Idriss, D. Stacchiola, J.C. Hanson, J.A. Rodriguez, Journal of Catalysis 291 (2012) 117–126.
[23] L.Y. Gan, R. Tian, X.B. Yang, D.H. Lu, Y. Zhao, Journal of Physical Chemistry C 116 (2012) 745–752.
[24] V.M. Shinde, G. Madras, Applied Catalysis B: Environmental 123–124 (2012) 367–378.
[25] E.B. Fox, S. Velu, M.H. Engelhard, Y.H. Chin, J.T. Miller, J. Kropf, C. Song, Journal of Catalysis 260 (2008) 358–370.
[26] J. Kugai, J.T. Miller, N. Guo, C. Song, Applied Catalysis B: Environmental 105 (2011) 306–316.
[27] Y. Li, Q. Fu, M. Flytzani-Stephanopoulos, Applied Catalysis B: Environmental 27 (2000) 179–191.
[28] S.C. Huang, C.H. Lin, J.H. Wang, Journal of Physical Chemistry C 114 (2010) 9826–9834.
[29] L.P.R. Profeti, E.A. Ticianelli, E.M. Assaf, International Journal of Hydrogen Energy 34 (2009) 5049–5060.
[30] M.H. Youn, J.G. Seo, P. Kim, J.J. Kim, H.I. Lee, I.K. Song, Journal of Power Sources 162 (2006) 1270–1274.
[31] K.R. Kim, S.W. Paek, H.J. Choi, H. Chung, Industrial & Engineering Chemistry Research 7 (2001) 116–120.
[32] C.N. Costa, A.M. Efstathiou, Applied Catalysis B: Environmental 72 (2007) 240–252.
[33] M. García-Mota, B. Bridier, J. Pérez-Ramírez, N. López, Journal of Catalysis 273 (2010) 92–102.
[34] Y.H. Kim, J.E. Park, H.C. Lee, S.H. Choi, E.D. Park, Applied Catalysis B: Environmental 127 (2012) 129–136.
[35] V.M. Shinde, G. Madras, Catalysis Today (2012) doi:10.1016/j.cattod.2012.02.019.
[36] P. Girault, J. Grosseau-Poussard, J. Dinhut, L. Marechal, Nuclear Instruments and Methods in Physics Research Section B: Beam Interactions with Materials and Atoms 174 (2001) 439–452.
[37] J.C. Fuggle, F.U. Hillebrecht, R. Zeller, Z. Zo1nierek, P.A. Bennett, Physical Review B 27 (1982) 2145–2178.
[38] P.A. Deshpande, M.S. Hegde, G. Madras, Applied Catalysis B: Environmental 96 (2010) 83–93.
[39] K. Priolkar, P. Bera, P. Sarode, M.S. Hegde, S. Emura, R. Kumashiro, N. Lalla, Chemistry of Materials 14 (2002) 2120–2128.
[40] D.R. Penn, Journal of Electron Spectroscopy and Related Phenomena 9 (1976) 29–40.
[41] J. Scofield, Journal of Electron Spectroscopy and Related Phenomena 8 (1976) 129–137.
[42] R. Leppelt, B. Schumacher, V. Plzak, M. Kinne, R. Behm, Journal of Catalysis 244 (2006) 137–152.
[43] A. Valentini, N.L.V. Carreño, L.F.D. Probst, A. Barison, A. Ferreira, E.R. Leite, E. Longo, Applied Catalysis A: General 310 (2006) 174–182.
[44] A. Trovarelli, Catalysis Reviews. Science and Engineering 38 (1996) 439–520.
[45] C. Wheeler, A. Jhalani, E. Klein, S. Tummala, L. Schmidt, Journal of Catalysis 223 (2004) 191–199.
[46] C. Rhodes, G. Hutchings, A. Ward, Catalysis Today 23 (1995) 43–58.
[47] L. Barrio, A. Kubacka, G. Zhou, M. Estrella, A. Martinez-Arias, J.C. Hanson, M. Fernandez-Garcia, J.A. Rodriguez, Journal of Physical Chemistry C 114 (2010) 12689–12697.
[48] K.R. Hwang, C.B. Lee, J.S. Park, Journal of Power Sources 196 (2011) 1349–1352.
[49] B.S. Caglayan, A.E. Aksoylu, Turkish Journal of Chemistry 33 (2009) 249–256.
[50] A.A. Phatak, K.M. Lee, P. Figaro, S. Rai, G. Zhu, K.T. Thomson, W.N. Delgass, F.H. Ribeiro, Annual Meeting Cincinnati, OH, 2005.
[51] C.M. Kalamaras, I.D. Gonzalez, R.M. Navarro, J.L.G. Fierro, A.M. Efstathiou, Journal of Physical Chemistry C 115 (2011) 11595–11610.
[52] F. Meunier, D. Reid, A. Goguet, S. Shekhtman, C. Hardacre, R. Burch, W. Deng, M. Flytzani-Stephanopoulos, Journal of Catalysis 247 (2007) 277–287.
[53] G.G. Olympiou, C.M. Kalamaras, C.D. Zeinalipour-Yazdi, A.M. Efstathiou, Catalysis Today 127 (2007) 304–318.
[54] K. Azzam, I. Babich, K. Seshan, L. Lefferts, Applied Catalysis B: Environmental 80 (2008) 129–140.
[55] P. Graf, D. De Vlieger, B. Mojet, L. Lefferts, Journal of Catalysis 262 (2009) 181–187.
[56] C.M. Kalamaras, P. Panagiotopoulou, D.I. Kondarides, A.M. Efstathiou, Journal of Catalysis 264 (2009) 117–129.
[57] C.M. Kalamaras, G.G. Olympiou, A.M. Efstathiou, Catalysis Today 138 (2008) 228–234.
[58] D. Tibiletti, A. Goguet, F.C. Meunier, J.P. Breen, R. Burch, Chemical Communications 14 (2004) 1636–1637.
[59] C.M. Kalamaras, S. Americanou, A.M. Efstathiou, Journal of Catalysis 279 (2011) 287–300.
[60] P. Panagiotopoulou, D.I. Kondarides, Catalysis Today 112 (2006) 49–52.
[61] P.A. Deshpande, M.S. Hegde, G. Madras, AIChE Journal 56 (2010) 1315–1324.
[62] H. Zhu, Z. Qin, W. Shan, W. Shen, J. Wang, Journal of Catalysis 233 (2005) 41–50.
[63] G. Jacobs, U.M. Graham, E. Chenu, P.M. Patterson, A. Dozier, B.H. Davis, Journal of Catalysis 229 (2005) 499–512.
[64] M. Menetrey, A. Markovits, C. Minot, Surface Science 524 (2003) 49–62.
[65] J. Falconer, R. Madix, Surface Science 48 (1975) 393–405.